Supporting Information

Optical Microscopy Imaging of the Thermally-Induced Spin Transition and Isothermal Multi-stepped Relaxation in a Low-Spin Stabilized Spin-Crossover Material

Pradip Chakraborty*[†], Mouhamadou Sy[‡], Houcem Fourati[¶], Teresa Delgado[§],

Mousumi Dutta[†], Chinmoy Das[†], Céline Besnard[‖], Andreas Hauser[§], Cristian

Enachescu[#] and Kamel Boukheddaden*[¶]

[†]Department of Chemistry, Indian Institute of Technology Kharagpur, Kharagpur-

721302, India

[‡]Université Assane Seck de Ziguinchor, Département de Physique, LCPM, BP 523

Diabir, Ziguinchor 27000, Sénégal

[¶]Université Paris-Saclay, UVSQ, CNRS, GEMAC, 45 Avenue des Etats Unis 78035,

Versailles

[§]Département de Chimie Physique, Université de Genève, 30, Quai Ernest-Ansermet,

CH-1211 Genève 4, Switzerland

[‖]Laboratoire de Cristallographie, Université de Genève, 24, Quai Ernest-Ansermet,

CH-1211 Genève 4, Switzerland

[#]Faculty of Physics, Al. I. Cuza University, 700506 Iasi, Romania

*Corresponding Authors, E-mail: pradipc@chem.iitkgp.ac.in ;
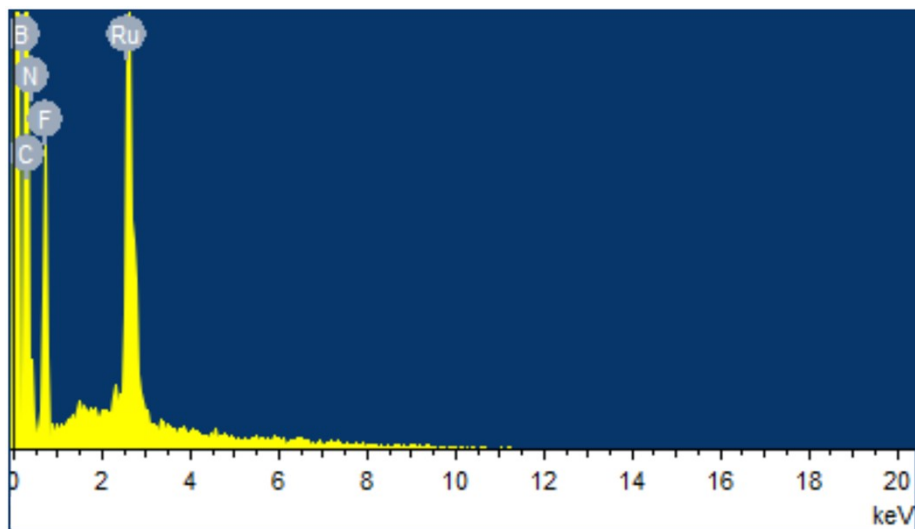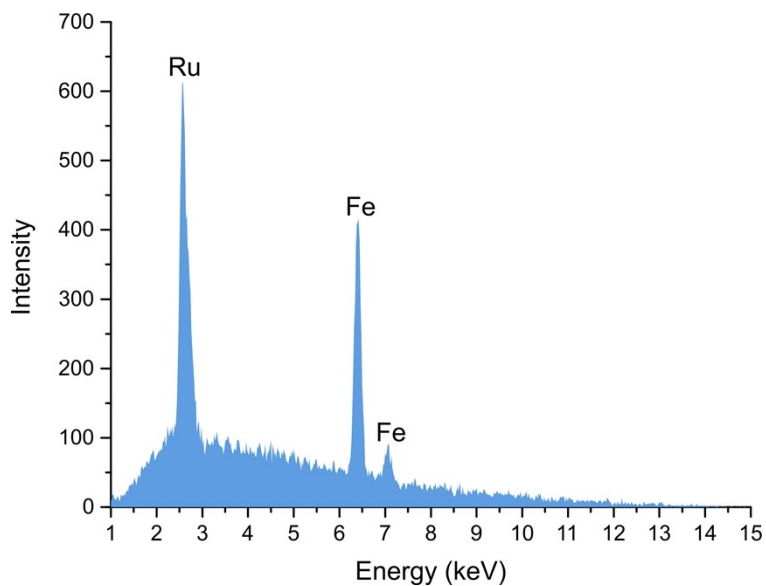
kamel.boukheddaden@uvsq.fr

Figure S1. EDX spectra of the mixed system $[Ru_{1-x}Fe_x(ptz)_6](BF_4)_2$ grown from a solution containing equimolar amount of Ru(II) and Fe(II) complex, resulting in an effective Fe(II) mole fraction of x = 0.65 (top panel) and crystals grown from a solution containing a Fe(II):Ru(II) ration of 1:10 in which within experimental accuracy no Fe(II) was incorporated (bottom panel).

Table S1. Energy-dispersive X-ray spectroscopy analysis of the representative concentration of Fe and Ru (in At. % and Atoms per formula unit).

Analysis	Fe (At. %)	Ru (At. %)	Fe (apfu)	Ru (apfu)
1	60.45	39.55	0.605	0.396
2	68.59	31.41	0.686	0.314
3	64.71	35.29	0.647	0.353
4	69.13	30.87	0.691	0.309
5	68.51	31.49	0.685	0.315
6	67.5	32.5	0.675	0.325
7	59.27	40.73	0.593	0.407
Mean	65.45	34.55	0.655	0.345

apfu = Atoms per formula unit

Crystallography
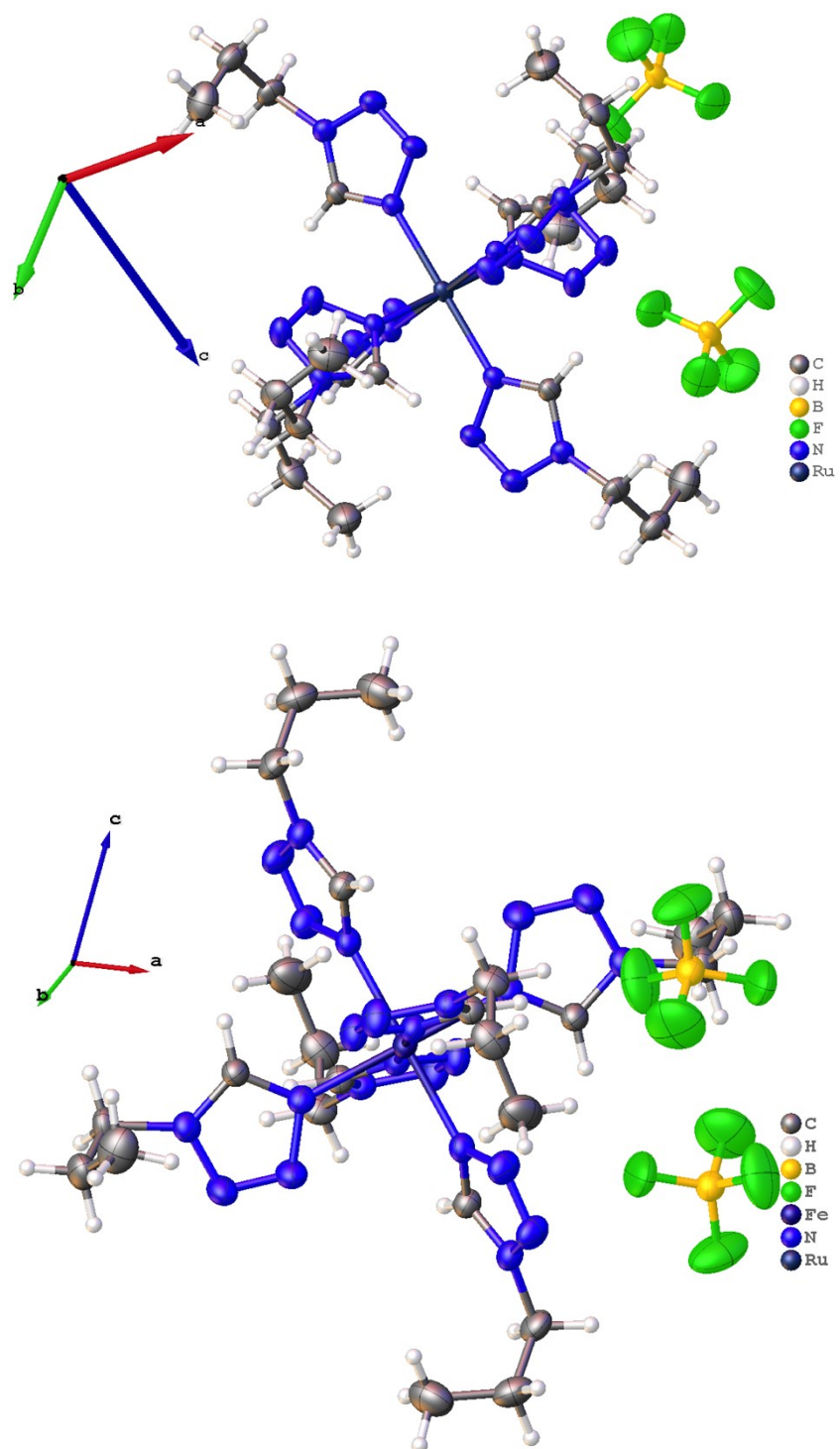
Figure S2. The entire structural unit of $[Ru(ptz)_6](BF_4)_2$ (Top) and of mixed $[Ru_{1-x}Fe_x(ptz)_6](BF_4)_2$ (Bottom) crystals at 150 K. Thermal ellipsoids are drawn at the 50% probability level.

Table S2. Crystal data and structure refinement for pure [Ru(ptz)$_6$](BF$_4$)$_2$ at 150 K.

Identification code	batch1_150K
Empirical formula	C24 H48 B2 F8 N24 Ru
Formula weight	947.55
Temperature	149(2) K
Wavelength	1.54184 Å
Crystal system	Trigonal
Space group	R -3
Unit cell dimensions	a = 10.79309(13) Å α = 90°
	b = 10.79309(13) Å β = 90°
	c = 32.1264(4) Å γ = 120°
Volume	3241.04(9) Å^3
Z	3
Density (calculated)	1.456 Mg/m^3
Absorption coefficient	3.694 mm^{-1}
F(000)	1458
Crystal size	0.367 x 0.256 x 0.234 mm^3
Theta range for data collection	4.128 to 74.287°.
Index ranges	-13<=h<=13, -12<=k<=12, -39<=l<=39
Reflections collected	8246
Independent reflections	1479 [R(int) = 0.0278]
Completeness to theta = 67.684°	99.9 %
Absorption correction	Gaussian
Max. and min. transmission	1.000 and 0.347
Refinement method	Full-matrix least-squares on F^2
Data / restraints / parameters	1479 / 0 / 91
Goodness-of-fit on F^2	1.059
Final R indices [I>2sigma(I)]	R1 = 0.0305, wR2 = 0.0814
R indices (all data)	R1 = 0.0305, wR2 = 0.0814
Extinction coefficient	n/a
Largest diff. peak and hole	0.736 and -0.575 e.Å^{-3}

Table S3. Crystal data and structure refinement pure [Ru(ptz)$_6$](BF$_4$)$_2$ at 80 K in the quenched, supercooled phase.

Identification code	batch1_80K_quenched
Empirical formula	C24 H48 B2 F8 N24 Ru
Formula weight	947.55
Temperature	81(2) K
Wavelength	1.54184 Å
Crystal system	Trigonal
Space group	R -3
Unit cell dimensions	a = 10.77425(13) Å $\quad$ $\square$= 90°
	b = 10.77425(13) Å $\quad$ $\square$= 90°
	c = 31.8415(5) Å $\quad$ $\square$ = 120°
Volume	3201.09(9) Å^3
Z	3
Density (calculated)	1.475 Mg/m^3
Absorption coefficient	3.740 mm^{-1}
F(000)	1458
Crystal size	0.367 x 0.256 x 0.234 mm^3
Theta range for data collection	4.165 to 74.166°.
Index ranges	-12<=h<=11, -13<=k<=13, -39<=l<=38
Reflections collected	12059
Independent reflections	1460 [R(int) = 0.0362]
Completeness to theta = 67.684°	99.8 %
Absorption correction	Gaussian
Max. and min. transmission	1.000 and 0.407
Refinement method	Full-matrix least-squares on F^2
Data / restraints / parameters	1460 / 0 / 91
Goodness-of-fit on F^2	1.084
Final R indices [I>2sigma(I)]	R1 = 0.0244, wR2 = 0.0589
R indices (all data)	R1 = 0.0244, wR2 = 0.0589
Extinction coefficient	n/a
Largest diff. peak and hole	0.370 and -0.568 e.Å^{-3}

Table S4. Crystal data and structure refinement for pure [Ru(ptz)₆](BF₄)₂ at 80 K on slowly cooled phase.

Identification code	batch 1_80K_slowcooled_tric
Empirical formula	C24 H48 B2 F8 N24 Ru
Formula weight	947.55
Temperature	80.0(5) K
Wavelength	1.54184 Å
Crystal system	Triclinic
Space group	P-1
Unit cell dimensions	$a = 11.7827(3)$ Å $\alpha = 90.9202(14)°$
	$b = 10.88012(19)$ Å $\beta = 99.0617(17)°$
	$c = 16.3802(3)$ Å $\gamma = 89.4706(17)°$
Volume	2073.38(7) Å^3
Z	2
Density (calculated)	1.518 Mg/m^3
Absorption coefficient	3.850 mm^{-1}
F(000)	972
Crystal size	0.283 x 0.216 x 0.162 mm^3
Theta range for data collection	2.732 to 74.193°.
Index ranges	-14<=h<=14, -13<=k<=13, -18<=l<=20
Reflections collected	47423
Independent reflections	8226 [R(int) = 0.0520]
Completeness to theta = 67.684°	98.6 %
Absorption correction	Gaussian
Max. and min. transmission	1.000 and 0.183
Refinement method	Full-matrix least-squares on F^2
Data / restraints / parameters	8226 / 0 / 538
Goodness-of-fit on F^2	1.091
Final R indices [I>2sigma(I)]	R1 = 0.0714, wR2 = 0.2117
R indices (all data)	R1 = 0.0820, wR2 = 0.2277
Extinction coefficient	n/a
Largest diff. peak and hole	2.949 and -1.569 e.Å^{-3}

Table S5. Crystal data and structure refinement for mixed [Ru$_{1-x}$Fe$_x$(ptz)$_6$](BF$_4$)$_2$ at 150 K

Identification code	RuFe batch 2_150K
Empirical formula	C24 H48 B2 F8 Fe0.66 N24 Ru0.34
Formula weight	917.71
Temperature	149.7(5) K
Wavelength	0.71073 Å
Crystal system	Trigonal
Space group	R -3
Unit cell dimensions	a = 10.8269(5) Å $\quad$ □= 90°
	b = 10.8269(5) Å $\quad$ □= 90°
	c = 32.0261(19) Å $\quad$ □ = 120°
Volume	3251.2(4) Å^3
Z	3
Density (calculated)	1.406 Mg/m^3
Absorption coefficient	0.438 mm^{-1}
F(000)	1422
Crystal size	0.4 x 0.317 x 0.067 mm^3
Theta range for data collection	3.764 to 28.149°.
Index ranges	-9<=h<=14, -13<=k<=11, -34<=l<=41
Reflections collected	7751
Independent reflections	1568 [R(int) = 0.0655]
Completeness to theta = 25.242°	99.7 %
Absorption correction	Gaussian
Max. and min. transmission	1.000 and 0.457
Refinement method	Full-matrix least-squares on F^2
Data / restraints / parameters	1568 / 0 / 92
Goodness-of-fit on F^2	1.054
Final R indices [I>2sigma(I)]	R1 = 0.0475, wR2 = 0.1129
R indices (all data)	R1 = 0.0604, wR2 = 0.1222
Extinction coefficient	n/a
Largest diff. peak and hole	0.775 and -0.558 e.Å^{-3}

Table S6. Crystal data and structure refinement for [Ru$_{1-x}$Fe$_x$(ptz)$_6$](BF$_4$)$_2$ at 80 K in the quenched, supercooled phase.

|	
Identification code	RuFe_batch2_80K_quenched_supercooled
Empirical formula	C24 H48 B2 F8 Fe0.66 N24 Ru0.34
Formula weight	917.71
Temperature	80.0(6) K
Wavelength	0.71073 Å
Crystal system	Trigonal
Space group	R -3
Unit cell dimensions	a = 10.7344(4) Å $\quad$ $\square$= 90°
	b = 10.7344(4) Å $\quad$ $\square$= 90°
	c = 32.0067(16) Å $\quad$ $\square$ = 120°
Volume	3193.9(3) Å^3
Z	3
Density (calculated)	1.431 Mg/m^3
Absorption coefficient	0.445 mm^{-1}
F(000)	1422
Crystal size	0.4 x 0.317 x 0.067 mm^3
Theta range for data collection	3.359 to 28.063°.
Index ranges	-12<=h<=11, -13<=k<=10, -33<=l<=40
Reflections collected	7566
Independent reflections	1552 [R(int) = 0.0311]
Completeness to theta = 25.242°	99.8 %
Absorption correction	Gaussian
Max. and min. transmission	1.000 and 0.503
Refinement method	Full-matrix least-squares on F^2
Data / restraints / parameters	1552 / 0 / 92
Goodness-of-fit on F^2	1.121
Final R indices [I>2sigma(I)]	R1 = 0.0301, wR2 = 0.0614
R indices (all data)	R1 = 0.0361, wR2 = 0.0640
Extinction coefficient	n/a
Largest diff. peak and hole	0.302 and -0.293 e.Å^{-3}
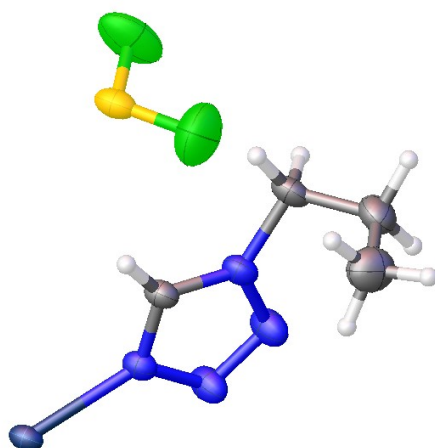
Figure S3: View of the asymmetric unit for pure [Ru(ptz)$_6$](BF$_4$)$_2$, at 150 K. Displacement parameters are shown at 50% probability level.

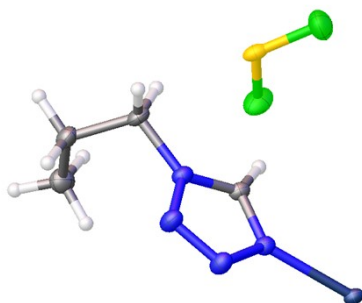**Figure S4:** View of the asymmetric unit for pure [Ru(ptz)$_6$](BF$_4$)$_2$, at 80 K (quenched, supercooled phase). Displacement parameters are shown at 50% probability level.

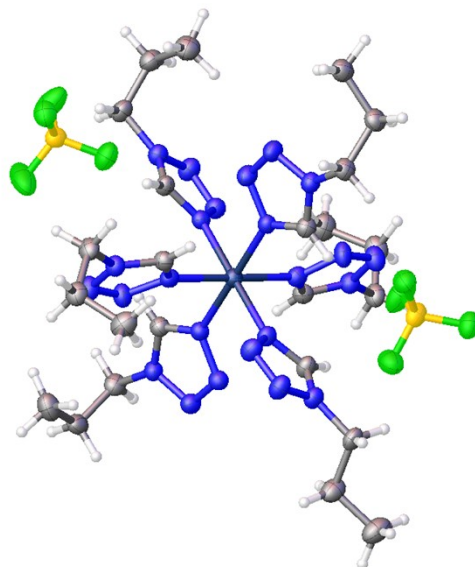**Figure S5:** View of the asymmetric unit for pure $[Ru(ptz)_6](BF_4)_2$, at 80 K (slowly cooled phase). Displacement parameters are shown at 50% probability level.
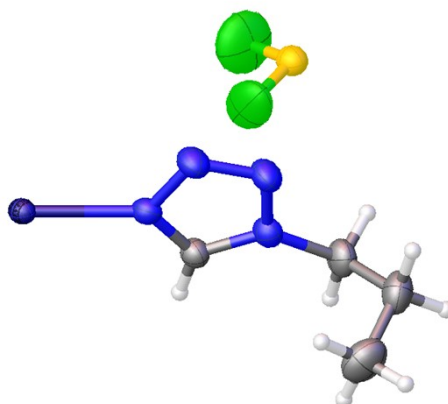
Figure S6: View of the asymmetric unit for mixed $[Ru_{1-x}Fe_x(ptz)_6](BF_4)_2$, at 150 K. Displacement parameters are shown at 50% probability level.
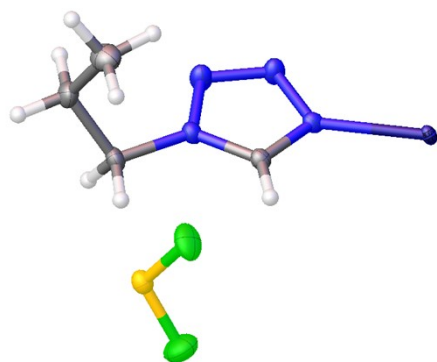
Figure S7: View of the asymmetric unit for $[Ru_{1-x}Fe_x(ptz)_6](BF_4)_2$ at 80 K (quenched, supercooled phase). Displacement parameters are shown at 50 percent probability level.
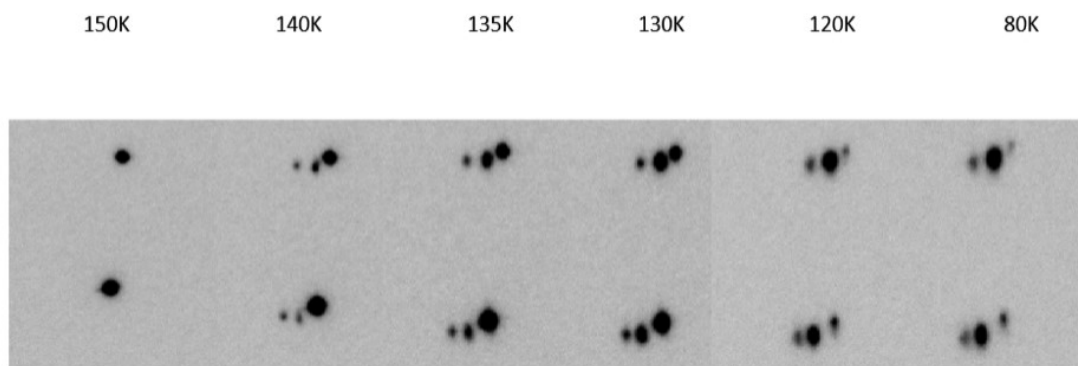
Figure S8: Evolution of the reflections as seen on the CCD camera with temperature (the two depicted reflections were indexed as (1, 2, -16) and (1, 1, -18) in the dataset of the crystal from mixed crystal).
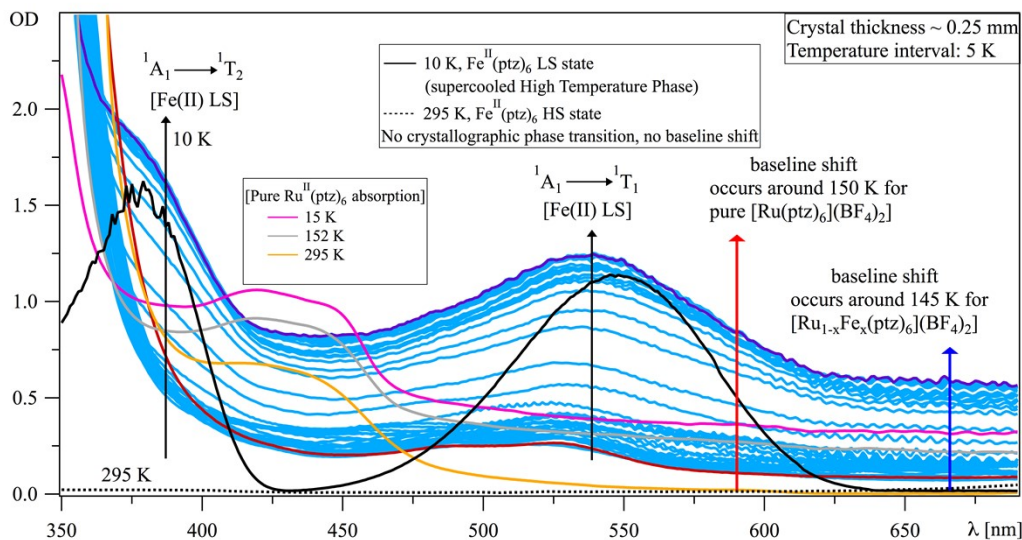
Figure S9. Comparison of the temperature-dependent single crystal (thickness ~ 0.25 mm) absorption spectra of pure $[Ru(ptz)_6](BF_4)_2$, mixed $[Ru_{1-x}Fe_x(ptz)_6](BF_4)_2$, $x = 0.65$ during the 1st cooling cycle, and pure $[Fe(ptz)_6](BF_4)_2$. For $[Ru(ptz)_6](BF_4)_2$ there is only one weak band centred at 425 nm, which doesn't show any significant evolution between 295 and 10 K. For $[Fe(ptz)_6](BF_4)_2$, the spectrum at 295 K (dotted black line), typical for the HS state, shows no absorption in the visible. At 10 K the typical $^1A_1 \rightarrow {}^1T_1$ and $^1A_1 \rightarrow {}^1T_2$ d-d transition typical for the LS state appear (solid black line). For mixed $[Ru_{1-x}Fe_x(ptz)_6](BF_4)_2$, the 295 K and the 10 K spectra are shown in red and purple, respectively. The intermediate spectra in light blue were taken in intervals of 5 K and show the increase in intensity of the $^1A_1 \rightarrow {}^1T_1$ transition typical for spin crossover. The characteristic transitions and temperature gradient are indicated by upward black arrows. A baseline shift towards lower temperature for $[Ru_{1-x}Fe_x(ptz)_6](BF_4)_2$ and pure $[Ru(ptz)_6](BF_4)_2$ are indicated by a blue and red upward arrows respectively.
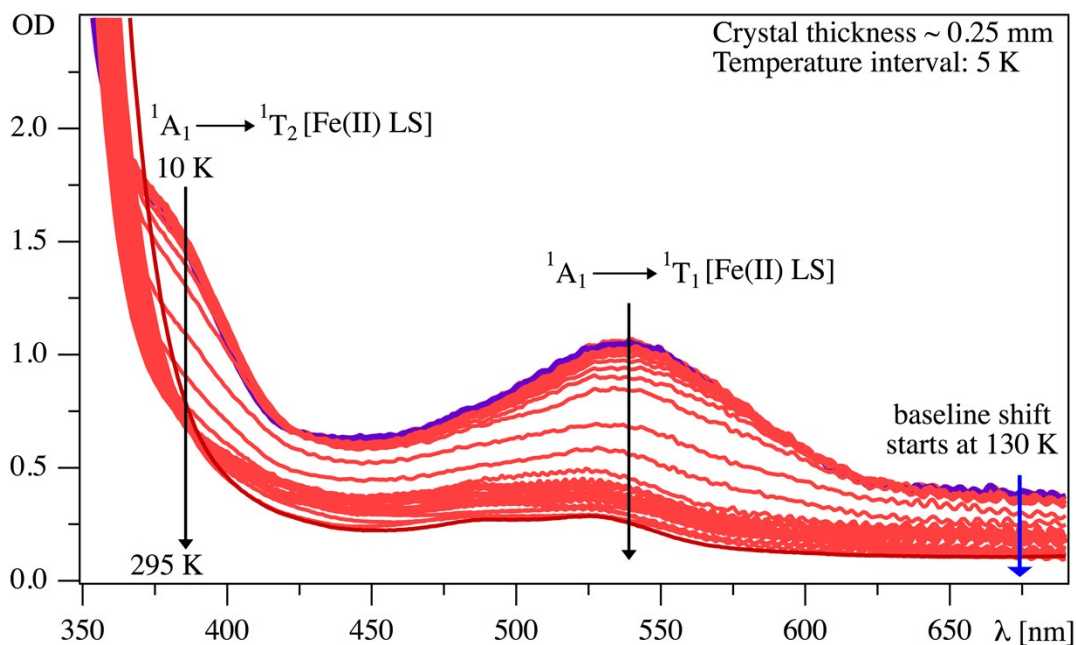
Figure S10. Single crystal (thickness ~ 0.25 mm) absorption spectra of $[Ru_{1-x}Fe_x(ptz)_6](BF_4)_2$, $x = 0.65$ as a function of temperature (every 5 K interval) with 0.2 K/min sweep rate from 10 K to 295 K during the 1st heating cycle. Purple and dark red spectra are shown for 10 K and 295 K respectively. All intermediate spectra are shown in light red. Downward black arrows indicate the characteristic transitions and temperature gradient. A baseline shift towards higher temperature is indicated by blue downward arrow.
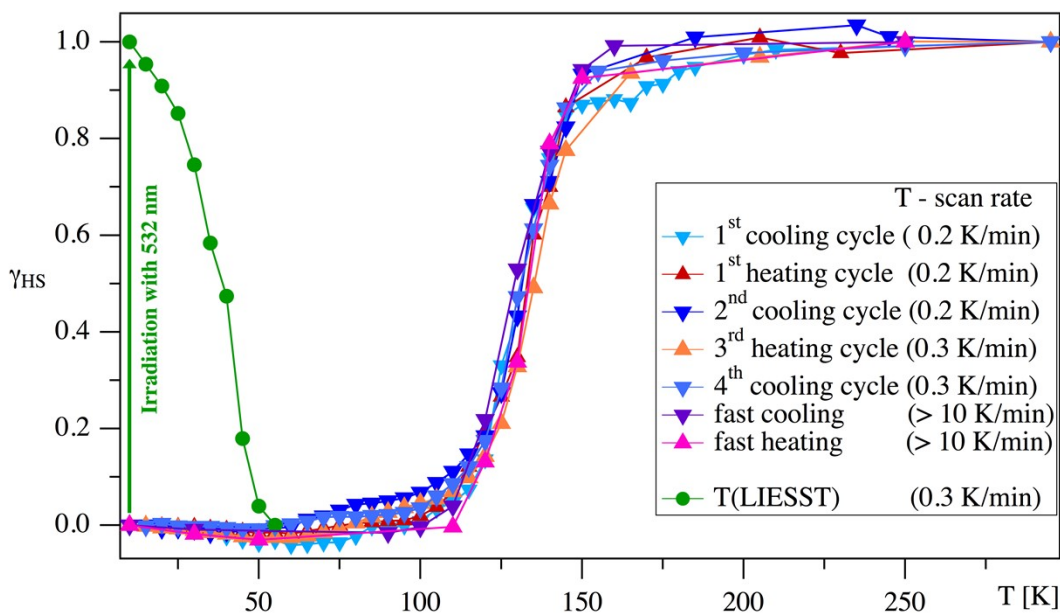
Figure S11. Thermal spin transition curves for $[Ru_{1-x}Fe_x(ptz)_6](BF_4)_2$, $x = 0.65$ obtained from optical absorption spectroscopy during 1st cooling cycle (sky blue downward solid triangles, temperature scan rate of 0.2 K per min), 1st heating cycle (red upward solid triangles, temperature scan rate of 0.2 K per min), 2nd cooling cycle (dark blue downward solid triangles, temperature scan rate of 0.2 K per min), 3rd heating cycle (orange upward solid triangles, temperature scan rate of 0.3 K per min), 4th cooling cycle (light blue downward solid triangles, temperature scan rate of 0.3 K per min), fast cooling (purple downward solid triangles) and fast heating (pink upward solid triangles) with temperature scan rate > 10 K per min. T(LIESST) curve (green filled circles) after irradiation with 532 nm at 10 K (green upward arrow) and heating with a temperature scan rate of 0.3 K per min

Optical microscopy

Determination of the HS fraction from optical microscopy data

The thermal dependence of the HS fraction, γ_{HS}, is derived from the spatially averaged renormalized optical density, $<OD>$, measured on a spatially-extended area of the crystal, excluding the borders at which strong light diffusion occurs. Assuming a linear relation between the HS fraction, γ_{HS}, and $<OD>$, leads to $\gamma_{HS}(T) = \dfrac{<OD>_T - <OD>_{LS}}{<OD>_{HS} - <OD>_{LS}}$, where $<OD>(T)$ stands for the spatial average optical density at temperature T, and $<OD>_{HS}$ and $<OD>_{LS}$ are those of LS and HS states, respectively. The spatial average of the optical density, is calculated as $<OD>_T = \dfrac{1}{S}\iint dx\, dy\, OD(x,y)$, where S is the crystal surface and $OD(x,y)$ is the local optical density at the pixel of coordinates (x,y), which is derived from the spatial cartography of the transmitted intensities, $I_T(x,y)$, through the crystal.

Comparison in the behavior of two different crystals

Let us now briefly discuss the possible origin of the small differences between thermal hysteresis behaviors derived from optical absorption (Figure 2) and OM (Figure 3c). First, as mentioned above for OM measurements, the thermal response is here also crystal-dependent. In addition to the previous aspects of shape and microstructures effects, the inhomogeneity of Ru concentration from one single crystal to another, may also play an important role, as it influences the volume change at the transition. Moreover, even if one assumes the same concentration of Ru between single crystals, there will be large microscopic spatial configurations of Ru distribution inside the crystals. Indeed, for a lattice with N Fe sites, assuming a random substitution of 50% Fe

16

sites by Ru leads to the large number, $\dfrac{N!}{\left(\dfrac{N}{2}!\right)^2}$, possible configurations. This inhomogeneous spatial distribution of Ru concentration inside the crystal, is an additional source of disorder which impacts the thermal properties of the material, making the results highly crystal dependent, particularly in the case where the substituents tend to aggregate.

To check this last point, we performed OM studies on cooling and heating in the temperature range 80-150 K on two other single crystals taken from the same batch as that of Figure 3. The results are summarized in Figure S12. The selected single crystals have different shapes and sizes. We denoted as **1** the pentagonal-shaped crystal and **2** the other big crystal for which we have only a partial view. Figures S12a and S12b present some selected snapshots for the heating and cooling processes, respectively, for both crystals **1** and **2**. The corresponding movies S3 and S4, respectively related to heating and cooling regimes, are also given in the SI. Figure S12c and Fig. S12d summarize the respective thermal dependences of the green OD of crystal **1** and **2,** obtained with a temperature scan rate of 1 K/min. In accordance with data of Fig. 3 and related movies S1 and S2, we do not see a strong visible front transformation in crystals **1** and **2** during their transitions, when we inspect the movies S3 and S4 (provided in the SI).

The case of crystal **1** is interesting and deserves a closer examination. In this crystal, whose snapshots are presented in Fig. S12a and S12b, we denoted A (image at 80 K in the LS state) the right corner which is used here as reference point. During the heating regime (Fig. S12a, movie S3), the global OD of the crystal slightly decreases in the region 130 -140 K (transmitted intensity increased) indicating the occurrence of a spin transition (Figure S12c) without any crystal motion or deterioration. On cooling however

17

(Fig. S12b, movie S4) a sudden crystal hopping out of the field of the camera takes place at $T = 121$ K, although we see a part of it in the top right corner of the image. As a result, the corresponding OD signal (Fig. S12c) falls to zero. This crystal jump is attributed to the mechanical stresses generated by the macroscopic volume contraction accompanying this spin transition. Interestingly, at 111 K, movie S4 shows, in a spectacular and unexpected way, the crystal coming back. This event is also well evidenced in the OD signal which jumps from zero to a non-null value (Fig. S12c). A meticulous inspection of the crystal shape indicates that (i) the reference point A changed a place and (ii) the light scattering at the borders has significantly decreased. This last point enables to conclude that the crystal hopping was accompanied with a self-cleaving, which is highly expected due to the polymeric nature of samples. On the other hand, the reappearance of the crystal after 10 K (from 121 K to 111 K) might be attributed to the "time" or temperature interval needed to complete its transformation, or to release the accumulated stresses, although this explanation remains at the moment quite hypothetical. It should nevertheless be pointed out that the case of jumping crystals was already detected at least once in SCO materials[68] and is quite familiar in organic/organometallic thermosalient crystals[69] whose phase transition cause their jumping by several centimeters or cracking, rotation and explosion.

The case of the big crystal **2,** which keeps its position during the whole study, is more common. The thermal dependence of its HS fraction, depicted in Figure S12d, shows a typical large thermal hysteresis of ~ 12 K width (comparable to that of Feptz), with upper and lower switching temperatures of 137 K and 125 K, in quite good agreement with those of crystal **1**. Interestingly, the average transition temperature, $T_{1/2} = 128$ K, is

slightly higher than that of Feptz ($T_{1/2} = 125\ K$), but remains lower than of the first studied crystal (132.5 K), which may be attributed to different Ru concentrations of the crystals.
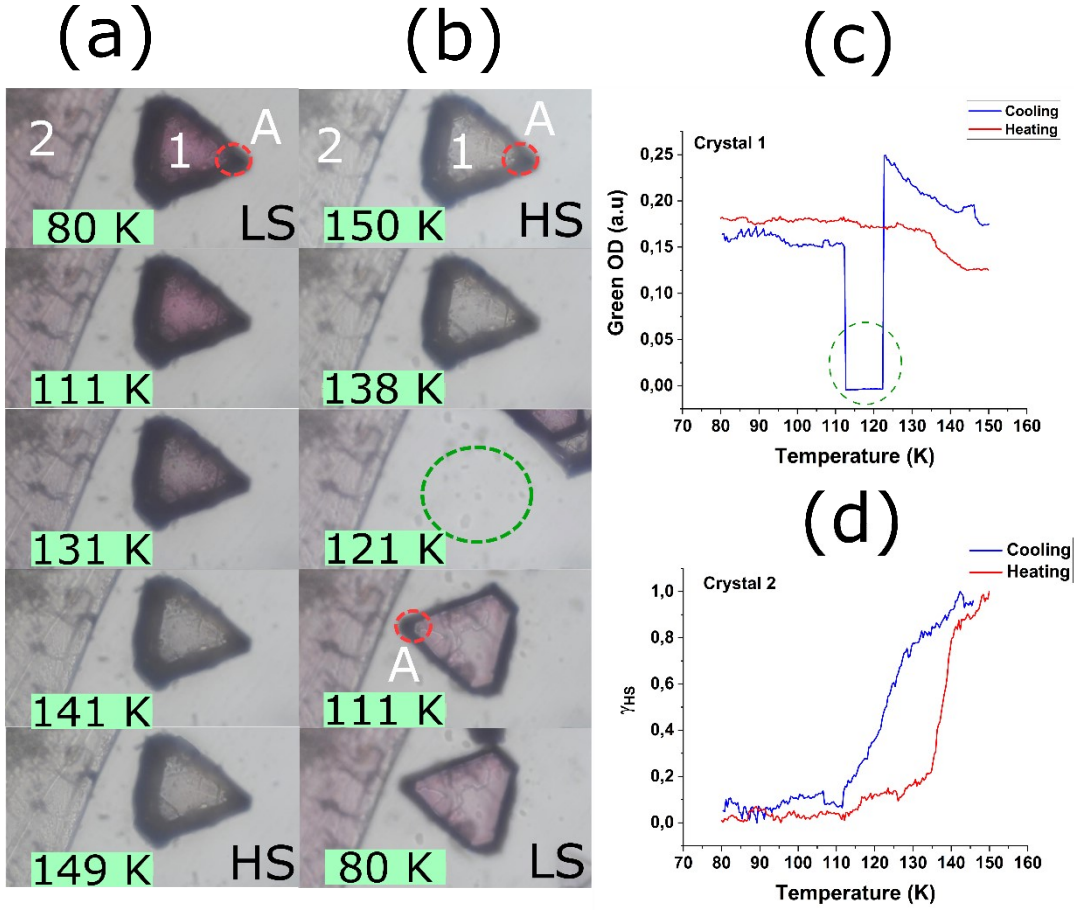

Figure S12: Selected snapshots showing the spatiotemporal behavior of transmission images of the crystal $[Ru_{1-x}Fe_x(ptz)_6](BF_4)_2$ (with $x = 0.65$) for two single crystals denoted here **1** (pentagonal shape) and **2** (whose a large part goes beyond the field of the visible part) during the spin transition for (a) the heating and (b) cooling branches of the thermal hysteresis, recorded at scan rate $r = 1$ K/min. The dashed red circle denoted A (image at 80 K on cooling) is used as a visual reference to identify this particular corner of crystal **1.** Notice the jumping of crystal **1** out of the field of the microscope on heating at 121 K (see top right corner) and its coming back at 111 K after a "salto" (corner A is now in the left). – (c) Thermal dependences of the green OD of crystal **1** showing- a region [111-121K] with a null OD, corresponding the "period" where the crystal is out of the field of the microscope- (d) Thermal dependence of the HS fraction of crystal **2** derived from the spatially averaged OD, showing a thermal hysteresis around 125 K.

19

List of deposited movie files:

We have used the frequency sampling method that allows creating a filter based on a desired frequency response to enhance the contrast between the HS and LS phases. For that, we implemented the function fsamp2 of Matlab, to realize this frequency sampling design for two-dimensional FIR (finite impulse response) filters. The procedure returns a filter h with a frequency response that passes through the points in the input matrix H. We have developed a filter of 11 by 11 using fsamp2 and filter2 of Matlab software for the different pixels RGB (Red Green Blue) and we have monitored the H values to increase the luminosity and the matrix of the color channels. After image processing, we have used the print function to save the new images (size average $\sim 770 \times 590$ pixels) before to crop them with the density of 96 dpi.

Movie S1: Real time movie recorded under the microscope, showing the transformation of $[Ru_{1-x}Fe_x(ptz)_6](BF_4)_2$, $x = 0.65$ single crystal along the heating branch from LS to HS. The temperature scan rate is $r = 1\,K.min^{-1}$ and the shinning intensity of the optical microscope lamp is $100\,mW$.

Movie S2: Real time movie recorded under the microscope, showing the transformation of $[Ru_{1-x}Fe_x(ptz)_6](BF_4)_2$, $x = 0.65$ single crystal on cooling from HS to LS. and the transition temperature is ~133 K. The temperature scan rate is $r = 1\,K.min^{-1}$ and the shinning intensity of the optical microscope lamp is $100\,mW$.

Movie S3: Optical microscopy visualization of the spatiotemporal transformation of crystals **1** (pentagonal shape) and **2** (big crystal) **of** $[Ru_{1-x}Fe_x(ptz)_6](BF_4)_2$, $x = 0.65$ on heating along the LS to HS transition in the temperature interval 80-150 K. The used temperature scan rate is, $r = 1\,K.min^{-1}$ and the shinning intensity of the optical microscope lamp is $100\,mW$. The transformation starts from the bulk.

Movie S4: Optical microscopy visualization of the spatiotemporal transformation of crystals **1** (pentagonal shape) and **2** (big crystal) **of** $[Ru_{1-x}Fe_x(ptz)_6](BF_4)_2$, $x = 0.65$ on heating along the LS to HS transition in the temperature interval 150-80 K. The temperature scan rate is $r = 1\,K.min^{-1}$ and the shinning intensity of the optical microscope lamp is $100\,mW$. The transformation appeared at the crystal borders. The crystal **1** jumps at 121 K leaves the field of the microscope and then comes back at 112.3 K.

O.D. fluctuations

Figure 3c of the main manuscript and Figs. S12 exhibit that the OD signal of the material is affected by the presence of fluctuations whose amplitude seem to be clearly independent on temperature, which suggest that they originate from the fluctuations of the incident intensity of the microscope rather than from the material properties. To clarify this origin, we performed the statistical analysis of this noise, and show below that this random noise affecting OD response follows a Gaussian distribution. For that, we first calculate the average optical density along the heating and cooling processes

$\ll OD \gg_i = \dfrac{<OD>_i + <OD>_{i+1}}{2}$ (the temperature is given by $T = T_0 + i \times \delta T$), from which we could derive the amplitude of the fluctuations, $\Delta OD_i = <OD>_i - \ll OD \gg_i$. The dependences of ΔOD_i with $<OD>_i$ for the cooling and heating regimes associated with Fig. 3 of the main manuscript are presented in Figs. S13 and S14, respectively with their corresponding histograms, which display a hard proof of the Gaussian distribution of the fluctuations of the OD. The probability density function for this normal distribution is:

$f(x,\mu,\sigma) = \dfrac{1}{\sigma\sqrt{2\pi}} exp[-\dfrac{(x-\mu)^2}{2\sigma^2}].$

Where $x = \Delta OD$, $\mu = <\Delta OD> \simeq 0$ and σ is the standard deviation, whose value is found here to be $\sigma = 0.001$ for both heating and cooling processes. The independence of the distribution on the history of the experiment (cooling/heating) indicates that the present fluctuations result from the random fluctuations of the light intensity of the microscope's lamp.
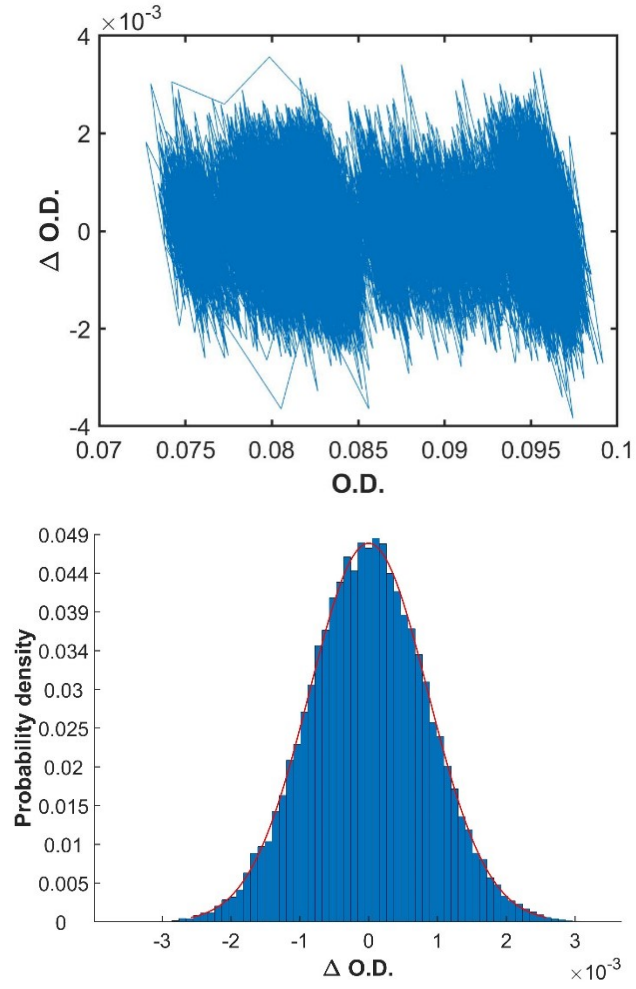
Figure S13: Upper panel: the amplitude of the OD fluctuations as function as the OD along the cooling branch of the thermal hysteresis of Fig. 3c. Lower panel: corresponding histogram of the OD fluctuations showing a Gaussian distribution.
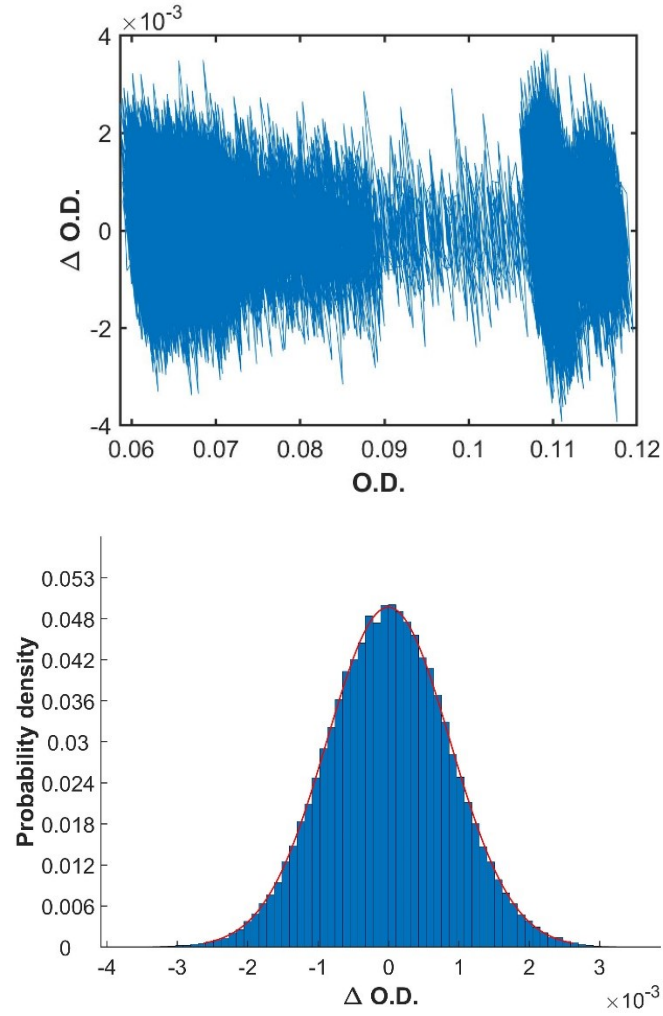
Figure S14: Upper panel: the amplitude of the OD fluctuations as function as the OD along the heating branch of the thermal hysteresis of Fig. 3c Lower panel: corresponding histogram of the OD fluctuations showing a Gaussian distribution.

Photo-induced HS → LS relaxation behavior

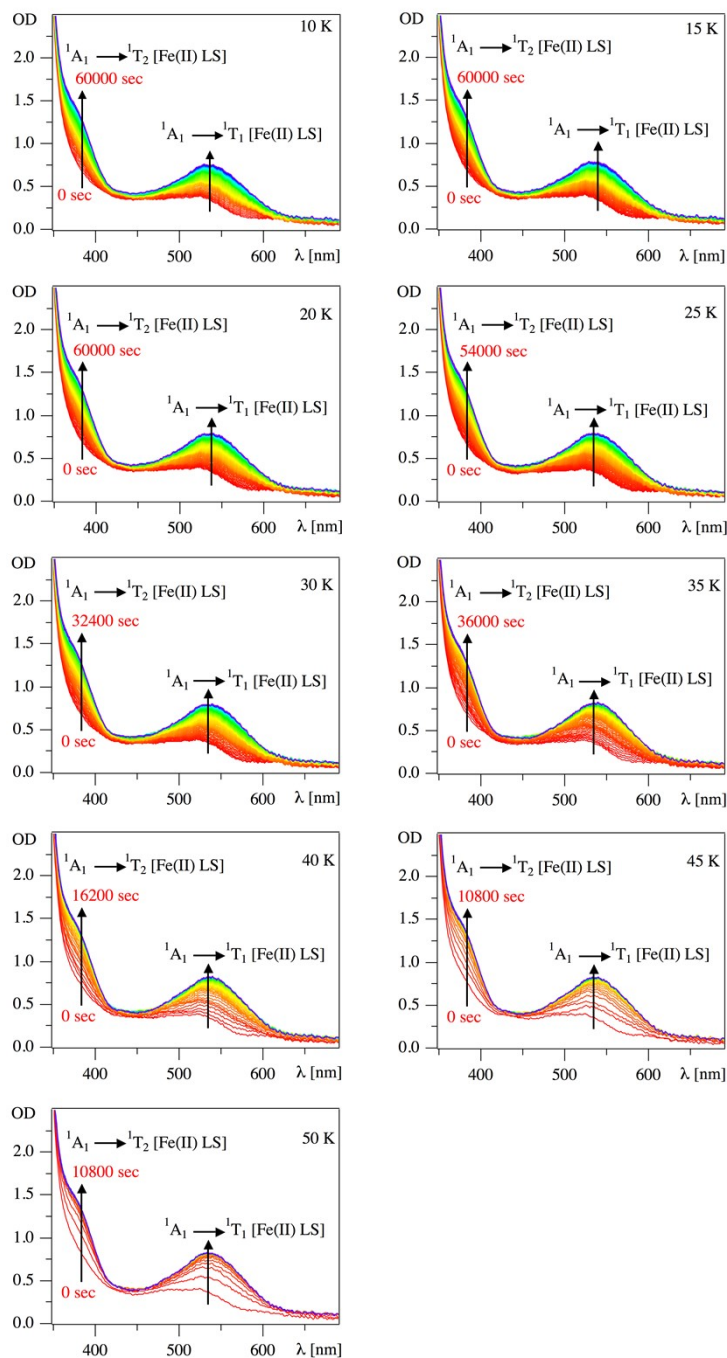**Figure S15.** Evolution of the single crystal absorption spectra during the photo-induced HS → LS relaxation as a function of temperature after irradiation with 532 nm (LIESST) at a nominal laser power of 2 mW. Each panel shows the evolution of the LS band intensities (*i.e.* $^1A_1 \rightarrow {}^1T_1$ and $^1A_1 \rightarrow {}^1T_2$ bands) as a function of time.

In Figure S16, we present the logarithmic representation for all curves between 10 and 35 K. We cannot apply this procedure for relaxation curves at temperature higher than 40 K as the relaxations are too fast and there are not enough points to properly compute the logarithm. In table S7 one shows the value of the self-acceleration parameters, as identified by this procedure. The average value of the self-acceleration parameter corresponds to a cooperative compound for all the described situations and the fluctuations are in the range of experimental errors.
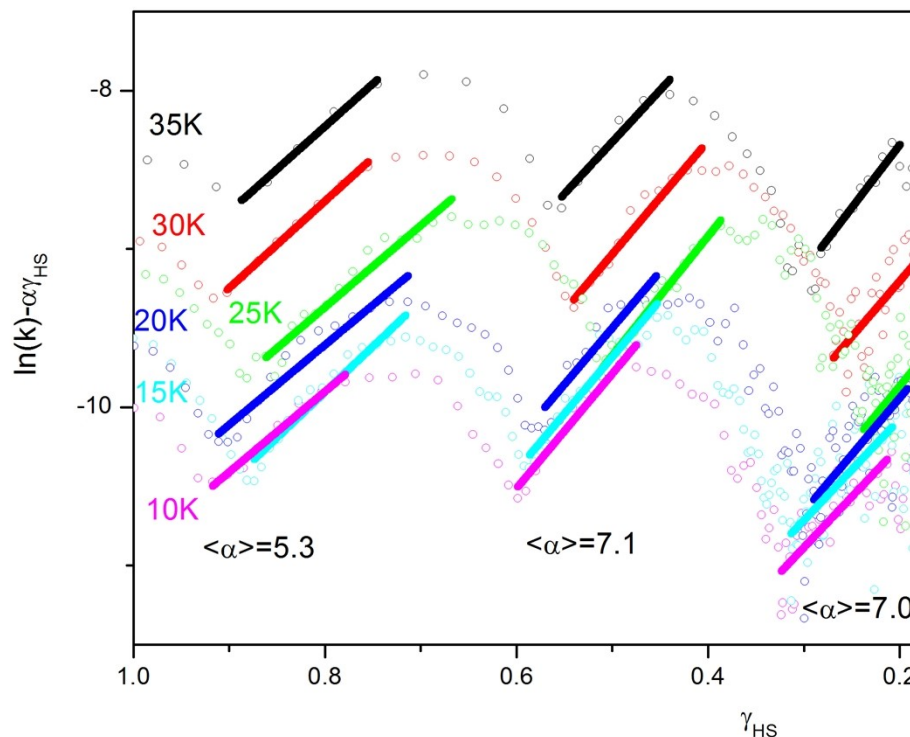

Figure S16: Logarithmic representation for curves between 10 and 35 K.

T	α_1	α_2	α_3
10	5.08	7.24	6.39
15	5.75	7.18	6.38
20	5.04	7.13	7.16
25	5.16	7.54	7.32
30	5.49	7.15	7.03
35	5.39	6.55	7.93
$\bar{\alpha}$	5.3	7.1	7.0

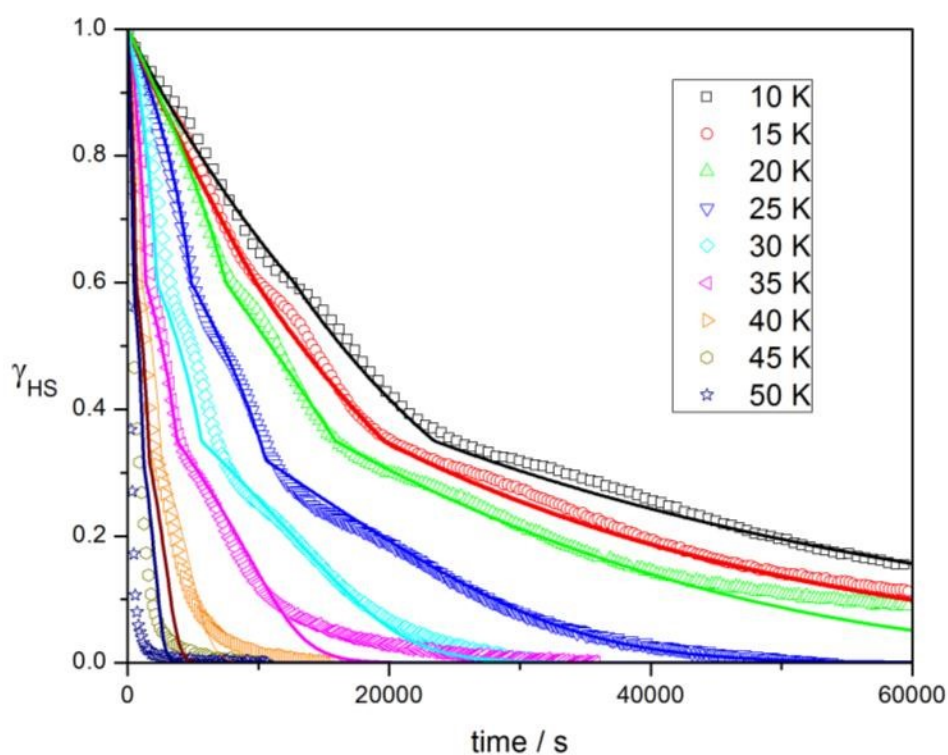**Table S7:** Interaction parameter α for every temperature and for every phase (relaxation part) and their average value.

Figure S17. Experimental relaxation and simulations for $[Ru_{1-x}Fe_x(ptz)_6](BF_4)_2$ compound at various temperatures. Experimental data (open symbols), simulations (solid curves).